

Mitigating Unbalanced GDoP Effects in Range-Based Vehicular Cooperative Localization

G.M. Hoang^{†‡}, B. Denis[†], J. Härrri[‡], D. T.M. Slock[‡]

[†]CEA-Leti, MINATEC Campus, 17 avenue des Martyrs, 38054 Grenoble, France

[‡]EURECOM, SophiaTech Campus, 450 route des Chappes, 06904 Biot, France

E-mails: {giaminh.hoang, benoit.denis}@cea.fr, {jerome.haerri, dirk.slock}@eurecom.fr

Abstract—In the context of Vehicular Ad Hoc NETWORKS (VANETs), we investigate the problem of range-based Cooperative Localization (CLoc), which combines *absolute* position information from on-board Global Navigation Satellite System (GNSS) with *relative* distance measurements to fellow mobile vehicles, for instance based on Impulse Radio - Ultra WideBand (IR-UWB). CLoc accuracy usually suffers from poor Geometric Dilution of Precision (GDoP) along the dimension orthogonal to the road, due to highly constrained VANET mobility and topology. This paper considers benchmarking and even combining two different approaches to resolve this problem. The first solution accounts for the vehicle’s heading, making use of an Inertial Measurement Unit (IMU). The second one assumes prior lane detection, along with associated road information (e.g., lane width stored in a digital map). The data fusion scheme is based on a modified Extended Kalman Filter (EKF) capable of filtering out the unbounded noise process integrated at the gyroscope and/or using lane boundaries to numerically refine the density of posterior state estimates. The proposed strategies are shown to boost the probability to reach an accuracy of 0.5 m from 60% up to 85–90% in comparison with conventional range-based approaches.

I. INTRODUCTION

In order to achieve the high positioning accuracy required by future Cooperative Intelligent Transport System (C-ITS) applications, new Cooperative Localization (CLoc) techniques suitable to Vehicular Ad hoc NETWORKS (VANETs) have been introduced recently. These solutions combine both Global Navigation Satellite System (GNSS) and “Vehicle-to-X” (V2X)¹ communication technologies. Accordingly, each “ego” vehicle considers its neighbors as potential “virtual anchors” [1]–[5] (i.e., mobile anchors with imperfect location information). Conceptually, CLoc follows three phases. First, each vehicle encapsulates its latest *absolute* location in a Beacon² broadcast over V2X communication links. Through the reception of such Beacons, a given “ego” vehicle thus becomes aware of the *absolute* positions of its neighbors. The second phase aims at retrieving *relative* Vehicle-to-Vehicle (V2V) location-dependent information with respect to “virtual anchors”, either out of received Beacon signals directly or by relying on a side ranging-enabled wireless technology. Ad hoc trilateration/triangulation can then be locally applied to fuse

the latter information with on-board GNSS position estimates and further refine the *absolute* location (See Fig. 1). In the last phase, the “ego” vehicle contributes to improve the localization of other vehicles by keeping on sharing its enhanced position estimates in subsequent Beacons.

CLoc has already been addressed rather extensively in [1], [3], [4], [6], exploiting signals of opportunity such as the Received Signal Strength Indicators (RSSI) of received Cooperative Awareness Messages (CAMs) [7], in compliance with V2X ITS-G5 technology³. However, RSSI-based ranging is a parametric technique that requires precise channel behavioral models. It is also very sensitive to channel irregularity and non-stationarity, including large fading dispersion or uncalibrated transmit power [1], [4], [8]. More recently, it has thus been proposed in [5] to replace ITS-G5-based RSSI measurements by Impulse Radio - Ultra WideBand (IR-UWB) Time-of-Flight (ToF) measurements, which can theoretically reach centimeter-level distance resolutions [8]. Nevertheless, despite the fine ranging potential of IR-UWB technology, the performance of fusion-based CLoc strongly depends on the geometric configuration of “virtual anchors”. In vehicular contexts, relative nodes positions are indeed strictly constrained by the topology of occupied roads/lanes and accordingly, they are unequally distributed along the road direction (along-track) and the direction orthogonal to the road (cross-track). Hence, the along-track location error can usually be significantly reduced, whereas the cross-track error cannot leverage ranging accuracy but mostly reveals poor Geometric Dilution of Precision (GDoP).

In this paper, we specifically aim at reducing cross-track errors by fusing GNSS positions and V2V IR-UWB range measurements with additional heading information issued at on-board Inertial Measurement Units (IMUs) or/and lane information (i.e., road geometry). One single data fusion framework based on a modified Extended Kalman Filter (EKF) is proposed, i) accounting for the uncertainties of “virtual anchors”, ii) mitigating the propagation of estimation biases through cooperative transactions, iii) reducing unbounded noise integrated at the gyroscope according to a prediction model and finally, iv) numerically refining the density of posterior

¹“V2X” refers to any technology capable of Device-to-Device (D2D) communication in a vehicular context.

²To remain technology neutral, a “Beacon” is a message periodically broadcast by each node.

³CAM and ITS-G5 are European counterparts to the Basic Safety Message (BSM) and Dedicated Short Range Communication (DSRC) in the US. ITS-G5 is expected to be available in every vehicle sold from 2019.

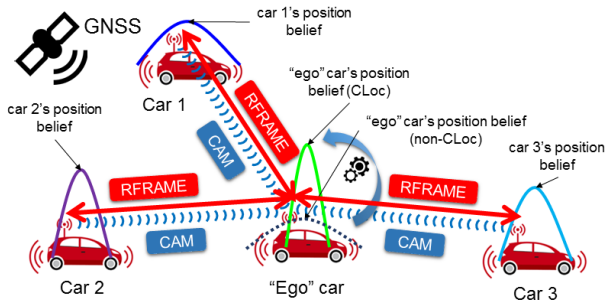


Fig. 1. “Ego” car receiving CAMs and exchanging ranging frames RFRAME from/with single-hop “virtual anchors” to perform distributed CLoc. The CLoc positional beliefs (i.e., after fusing GNSS and V2V IR-UWB ranges) are expected to be more concentrated than that of non-CLoc (i.e., with standalone GNSS only).

location estimates based on the knowledge of occupied lane’s boundaries, following an approach rather similar to [9].

The paper is organized as follows. Section II describes general concepts and system models related to CLoc, while Section III presents the main contributions of the paper. Simulation results and benchmarks are presented in Section IV. Finally, conclusions and future works are given in Section V.

II. PROBLEM FORMULATION

We consider a VANET consisting of a set \mathcal{V} of connected vehicles. At each vehicle $i \in \mathcal{V}$, time is locally sampled into a sequence of discrete events $t_{i,0}, t_{i,1}, \dots, t_{i,k}$, which are simply indexed by k^4 . Vehicles’ states are denoted by $\mathbf{X}_{i,k} = (\mathbf{x}_{i,k}^\dagger, \mathbf{v}_{i,k}^\dagger)^\dagger$, where $\mathbf{x}_{i,k} = (x_{i,k}, y_{i,k})^\dagger$, $\mathbf{v}_{i,k} = (v_{i,k}^x, v_{i,k}^y)^\dagger$ are the 2-D absolute position and 2-D velocity respectively. This state is assumed to evolve according to a mobility model. At discrete time $t_{i,k}$, the “ego” vehicle i has the set $\mathcal{S}_{\rightarrow i,k}$, $i \notin \mathcal{S}_{\rightarrow i,k}$ of “virtual anchors” and acquires an observation vector $\mathbf{z}_{i,k}$, which is related to its own state $\mathbf{X}_{i,k}$ and its neighboring states $\mathbf{X}_{j,k}$, $j \in \mathcal{S}_{\rightarrow i,k}$ via a measurement model.

A. True Mobility and Mobility Prediction Models Mismatch

For traffic simulations, we herein assume a Gauss-Markov mobility model, which describes well the correlated velocity of vehicles in the form of a time-correlated Gauss-Markovian process and is suitable into vehicular contexts [3], [10] i.e.,

$$\begin{aligned} \underbrace{\begin{pmatrix} \mathbf{x}_{i,k+1} \\ \mathbf{v}_{i,k+1} \end{pmatrix}}_{\mathbf{X}_{i,k+1}} &= \underbrace{\begin{pmatrix} \mathbf{I}_2 & \alpha \Delta T \mathbf{I}_2 \\ \mathbf{0}_2 & \alpha \mathbf{I}_2 \end{pmatrix}}_{\mathbf{F}(\alpha, \Delta T)} \underbrace{\begin{pmatrix} \mathbf{x}_{i,k} \\ \mathbf{v}_{i,k} \end{pmatrix}}_{\mathbf{X}_{i,k}} \\ &+ \underbrace{(1 - \alpha) \begin{pmatrix} \Delta T \mathbf{I}_2 \\ \mathbf{I}_2 \end{pmatrix}}_{\mathbf{B}(\alpha, \Delta T)} \underbrace{\bar{\mathbf{v}}_i}_{\mathbf{v}_i} + \underbrace{\sqrt{1 - \alpha^2} \begin{pmatrix} 1/2 \Delta T^2 \mathbf{I}_2 \\ \Delta T \mathbf{I}_2 \end{pmatrix}}_{\mathbf{G}(\alpha, \Delta T)} \mathbf{w}_{i,k}, \end{aligned} \quad (1)$$

where α is the memory level, ΔT the time step, $\bar{\mathbf{v}}_i = (\bar{v}_i^x, \bar{v}_i^y)^\dagger$ the 2-D asymptotic (cruising) velocity, $\mathbf{w}_{i,k} =$

⁴Due to asynchronously sampled time instants, the index k is locally meaningful. For notation brevity, the subscript indicating the vehicle index is dropped. If, however, it is included, the associated variable is strictly considered w.r.t. the timeline of the stated vehicle index.

$(w_{i,k}^x, w_{i,k}^y)^\dagger \sim \mathcal{N}((0, 0)^\dagger, \mathbf{Q}_{i,k})$ a 2-D Additive White Gaussian Noise (AWGN) term associated with noisy control inputs, \mathbf{I}_2 the identity matrix of size 2×2 .

Although we could assume that each vehicle has perfect knowledge about its own mobility model i.e., a model like in (1) or more generally, a conditional transition probability density function (pdf) $p(\mathbf{X}_{i,k+1} | \mathbf{X}_{i,k})$ (known *a priori* for highly controlled mobility regimes or possibly self-calibrated on the wing based on previous state estimates), this perception is usually an approximation of the true mobility statistics. To remain as mobility-independent as possible, one simpler approach consists in employing a very generic tracking model, e.g. a 2-D version of Newton’s force law [10], as mobility prediction model. The corresponding discrete time model is

$$\mathbf{X}_{i,k+1} = \underbrace{\begin{pmatrix} \mathbf{I}_2 & \Delta T \mathbf{I}_2 \\ \mathbf{0}_2 & \mathbf{I}_2 \end{pmatrix}}_{\tilde{\mathbf{F}}(\Delta T)} \mathbf{X}_{i,k} + \underbrace{\begin{pmatrix} 1/2 \Delta T^2 \mathbf{I}_2 \\ \Delta T \mathbf{I}_2 \end{pmatrix}}_{\tilde{\mathbf{G}}(\Delta T)} \tilde{\mathbf{w}}_{i,k}, \quad (2)$$

where $\tilde{\mathbf{w}}_{i,k} \sim \mathcal{N}((0, 0)^\dagger, \tilde{\mathbf{Q}}_i)$ is the 2-D process noise. It is important to keep the process noise covariance $\tilde{\mathbf{Q}}_i$ large enough so as to take into account the model’s prediction error (or model mismatch) and preserve filtering stability accordingly [11]. In practice, vehicle’s acceleration/deceleration capacity is used to fine-tune this process noise. Finally, this generic prediction model can be applied to any vehicle with simple tuning and is appropriate for predicting both “ego” and neighbors’ estimated states, as well as for resynchronizing related data before filtering/fusion⁵, like in [1], [3].

B. Observation Models

1) *GNSS Absolute Position*: The 2-D position estimate delivered by GNSS, $\mathbf{p}_{i,k} = (p_{i,k}^x, p_{i,k}^y)^\dagger$, is affected by an AWGN noise vector $\mathbf{n}_{i,k} = (n_{i,k}^x, n_{i,k}^y)^\dagger \sim \mathcal{N}((0, 0)^\dagger, \sigma_{\text{GNSS}}^2 \mathbf{I}_2)$ [2], [3] of standard deviation σ_{GNSS} .

$$p_{i,k}^x = x_{i,k} + n_{i,k}^x, \quad p_{i,k}^y = y_{i,k} + n_{i,k}^y. \quad (3)$$

2) *IR-UWB V2V Ranges*: Through a ranging protocol (e.g., based on the ToF estimation of transmitted packets involved in multiple-way handshake transactions [8], [12]), vehicle i at time $t_{i,k}$ estimates the V2V distance $\tilde{d}_{j \rightarrow i,k}$ to node j , $j \in \mathcal{S}_{\rightarrow i,k}$ in position \mathbf{x}_{j,k_i}

$$\tilde{d}_{j \rightarrow i,k} = \|\mathbf{x}_{i,k} - \mathbf{x}_{j,k_i}\| + n_{j \rightarrow i,k}, \quad (4)$$

where $n_{j \rightarrow i,k} \sim \mathcal{N}(0, \sigma_{\text{UWB}}^2)$ is the ranging measurement noise of standard deviation σ_{UWB} .

3) *IMU Heading*: The vehicle’s heading is obtained by integrating the yaw rate given by the rate-gyroscope of an IMU, given heading initialization⁶. The measured angular rate

⁵The transmission intervals between CAMs are constrained by channel load conditions, leading to non periodic transmissions and as such, non synchronous data reception from the “virtual anchors”. If a highly parametric mobility prediction is employed, model-specific parameters might not be supported by the standard 300-byte CAM.

⁶Heading can be initialized (at rest or in motion) using magnetic compass, gyrocompass, lane marker detection with an enhanced digital map, etc. with rather high accuracy of a few milliradians (a tenth of degree) [11], [13].

about the vertical axis $\tilde{\omega}_{i,k}^z$ at time $t_{i,k}$ is characterized by a general-purpose parametric model [11], [14], such as

$$\tilde{\omega}_{i,k}^z = (S + \delta S)\omega_{i,k}^z + b_{i,k}^{f,\omega} + b_{i,k}^{i,\omega} + n_{i,k}^\omega, \quad (5)$$

where S is the scale factor, δS the scale factor error, $\omega_{i,k}^z$ the true yaw rate, $b_{i,k}^{f,\omega}$, $b_{i,k}^{i,\omega}$ the fixed bias and bias instability respectively, $n_{i,k}^\omega$ the thermal noise. The scale factor and fixed bias are deterministic by nature and can be calibrated at sensor level [14], [15]. The bias instability refers to bias drift, typically modeled as a random walk [15], [16]. The vehicle's heading is determined by integrating the gyro signal, following the rectangular rule. Thus, the thermal noise and the bias instability result in angle random walk and second-order random walk in the integrated signal respectively. Using Allan Variance analysis, at 10 Hz⁷, thermal noise is the most important noise process perturbing the gyro signals [16]. Hence, the vehicle's heading measurement can be modeled as

$$\tilde{\theta}_{i,k} \approx \theta_{i,k} + b_{i,k}^\theta + \epsilon_{i,0}^\theta = \text{atan2}(v_{i,k}^y, v_{i,k}^x) + b_{i,k}^\theta + \epsilon_{i,0}^\theta, \quad (6)$$

where $\theta_{i,k}$ and $\tilde{\theta}_{i,k}$ denote the true and measured headings respectively, $\text{atan2}(y, x)$ the four-quadrant inverse tangent, $\epsilon_{i,0}^\theta \sim \mathcal{N}(0, (\sigma_{i,0}^\theta)^2)$ the heading initialization error, and $b_{i,k}^\theta$ the random walk term. The random walk error model has the following form

$$b_{i,k}^\theta = b_{i,k-1}^\theta + n_{i,k}^\theta, \quad (7)$$

where $n_{i,k}^\theta$ is a centered AWGN random term with standard deviation $\sigma_{i,k}^\theta \sqrt{\Delta T / B_i^\omega}$, where $\sigma_{i,k}^\omega$ is the standard deviation of the yaw rate signal for a bandwidth B_i^ω , and ΔT is the integrated timespan.

III. PROPOSED APPROACHES

A. Limitations of Range-Based CLoc in VANETs

In the VANET context, the performance of the range-based CLoc depends critically on three factors: (i) the quality of the range measurements, (ii) the uncertainties of the positions of the “ego” vehicle and its “virtual anchors”, and (iii) the local geometric configuration of the latter anchors relatively to the “ego” vehicle. The first factor can be satisfied by accurate time-based ranging via IR-UWB technology. The second factor can be taken into account in a modified EKF, capable of monitoring the uncertainties of the “virtual anchors” (See Algorithm 1) and by broadcasting enhanced position estimates so as to assist neighbors (similarly to message passing). Since mobility is strongly constrained by the roads/lanes and driving rules, the relative vehicles' geometry is rather poorly conditioned in this very context. Specifically, the VANET topology is usually somehow distorted along the direction colinear to the road due to the huge disparity between the longitudinal safety distances (e.g., 20–150 m⁸) and the lateral lane width (e.g., 2.25–3.5 m). Accordingly, the GDop is

⁷We consider in this paper 10-Hz tracking. Otherwise, at the speed of 110 km/h (30 m/s), 1-Hz tracking gives single position estimate per 30 m.

⁸The two-second (or three-second) rule is applied to maintain a safe following distance.

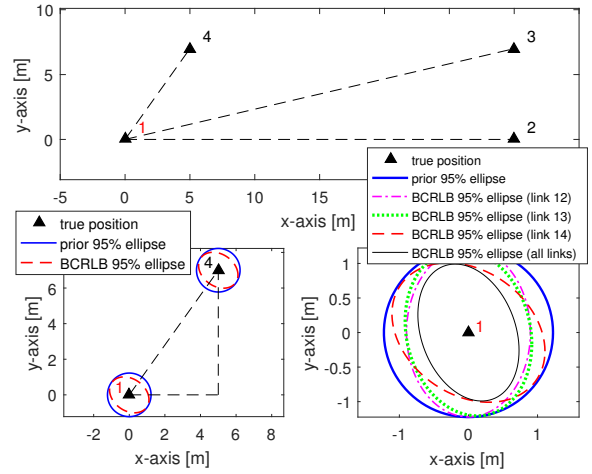


Fig. 2. Example of expected CLoc localization performance in a 4-node VANET. The top subfigure shows the true vehicles positions. The left bottom subfigure illustrates how a single range-based cooperative transaction mostly increases information (i.e., decreases confidence ellipse) in the direction formed by the two involved nodes' positions. The right bottom subfigure shows the impact of each link separately and of all links on the final “ego” localization performance. Main parameters include a prior $1-\sigma$ uncertainty of 1 [m] on both x - and y -coordinates independently and a ranging standard deviation $\sigma_{\text{UWB}} = 0.2$ [m].

likely poor in the direction orthogonal to the road; therefore, the cross-track location error remains high. The CLoc performance is illustrated for a given VANET on Fig. 2, where the expected positioning error level *before* (prior) and *after* cooperation is theoretically predicted using the Bayesian Cramér-Rao Lower Bound (BCRLB) [3] and represented as 95%-confidence ellipses. Fig. 2 (right bottom) also shows that vehicles maintaining safety distances to the “ego” (regardless of their lane occupancy) mainly improve “ego” along-track positioning whereas vehicles at closer range (obviously on different lanes) generally improve “ego” cross-track positioning. The latter are tightly constrained due to the limited number of lanes (2 or 3 in each direction for most common European roadways), regardless of V2V communication range. Hence, additional information having beneficial impact on the cross-track error must be fused in the GNSS+UWB CLoc.

B. IMU Heading Integration in Modified EKF-based Fusion

Intuitively, a high-quality gyroscope improves the heading error as well as the cross-track positioning error which CLoc cannot fully resolve. Thus we first propose to incorporate the vehicle's heading information measured by a gyroscope in the fusion-based CLoc. As aforementioned, the heading measurement error is modeled as a random walk process, whose overall variance grows linearly with time (see (7)). Thus this error must be estimated to get reliable filtering/fusion results. Said differently, we augment the state of the “ego” vehicle i as $\mathbf{X}_{i,k}^a := (\mathbf{X}_{i,k}^\dagger, b_{i,k}^\theta)^\dagger$. We then combine (2) and (7) to obtain an augmented prediction model as follow

$$\mathbf{X}_{i,k+1}^a = \underbrace{\begin{pmatrix} \tilde{\mathbf{F}}(\Delta T) & \mathbf{0} \\ \mathbf{0} & 1 \end{pmatrix}}_{\tilde{\mathbf{F}}^a(\Delta T)} \mathbf{X}_{i,k}^a + \underbrace{\begin{pmatrix} \tilde{\mathbf{G}}(\Delta T) & \mathbf{0} \\ \mathbf{0} & 1 \end{pmatrix}}_{\tilde{\mathbf{G}}^a(\Delta T)} \tilde{\mathbf{w}}_{i,k}^a, \quad (8)$$

where $\tilde{\mathbf{w}}_{i,k}^a = (\tilde{\mathbf{w}}_{i,k}^\dagger, n_{i,k}^\theta)^\dagger$, whose covariance matrix is

$$\tilde{\mathbf{Q}}_i^a(\Delta T) = \begin{pmatrix} \tilde{\mathbf{Q}}_i(\Delta T) & \mathbf{0} \\ \mathbf{0} & (\sigma_i^\omega)^2 \Delta T / B_i^\omega \end{pmatrix}. \quad (9)$$

Note that we consider EKF-based CLoc with mobile ‘‘virtual anchors’’, whose positions are not perfectly known, and a IR-UWB V2V range measurement model that depends on the positions of both ‘‘ego’’ and cooperative vehicles (See (4)). The ‘‘ego’’ state must be augmented once again to account for the states of the ‘‘virtual anchors’’ so that the corresponding augmented state covariance now includes the uncertainties of these ‘‘virtual anchors’’. Such state augmentation is vital to compute the adequate correction (i.e., to reduce the Kalman gain according to anchor’s uncertainty) for each V2V range measurement. Otherwise, the EKF treats ‘‘virtual anchors’’ as real anchors, and estimation biases in the neighboring estimates are propagated to the ‘‘ego’’ estimate, leading to significant accuracy degradation⁹.

We introduce the following set of notations to gather different vehicles’ variables: stacked states of ‘‘virtual anchors’’ $\mathbf{X}_{\mathcal{S} \rightarrow i,k} = \{\mathbf{X}_{j,k_i} | \forall j \in \mathcal{S} \rightarrow i,k\}$; new augmented state $\mathbf{X}_{i \cup \mathcal{S},k} = (\mathbf{X}_{i,k}^\dagger, \mathbf{X}_{\mathcal{S} \rightarrow i,k}^\dagger)^\dagger$; V2V ranges vector $\tilde{\mathbf{d}}_{\mathcal{S} \rightarrow i,k} = \{\tilde{d}_{j \rightarrow i,k} | \forall j \in \mathcal{S} \rightarrow i,k\}$; and full measurements vector

$$\mathbf{z}_{i,k} = \left(\mathbf{p}_{i,k}^\dagger, \tilde{\theta}_{i,k}, \tilde{\mathbf{d}}_{\mathcal{S} \rightarrow i,k} \right)^\dagger = \mathbf{h}_{i,k}(\mathbf{X}_{i \cup \mathcal{S},k}) + \mathbf{n}_{i,k}, \quad (10)$$

where $\mathbf{h}_{i,k}(\cdot)$ and $\mathbf{n}_{i,k}$ represent the mixed linear/nonlinear dependency of filter observation on the new augmented state and the measurement noise respectively (by combining (3), (6), and (4)). Assume various measurement noises are independent, the new noise covariance matrix is given as

$$\mathbf{R}_{i,k} = \begin{pmatrix} \sigma_{\text{GNSS}}^2 \mathbf{I}_2 & \mathbf{0} & \mathbf{0} \\ \mathbf{0} & (\sigma_{i,0}^\theta)^2 & \mathbf{0} \\ \mathbf{0} & \mathbf{0} & \sigma_{\text{UWB}}^2 \mathbf{I}_{|\mathcal{S} \rightarrow i,k|} \end{pmatrix}. \quad (11)$$

The overall proposed EKF-based fusion scheme integrating GNSS, IR-UWB and IMU, is described in Algorithm 1.

C. Lane Constraints (LC) Integration

As already mentioned, the mobility of land vehicles is tightly constrained by the road and lane boundaries. Thus, such contextual information can be contributed into the localization problem [11]. We assume in this paper that lane allocation can be performed at each vehicle using for instance a vision-based system (e.g., monocular camera) and a digital map [17]. The latest filtered/fused estimate is cross-checked with the side digital map to identify the current road occupancy and its associated attributes (e.g., lanes number and width). In addition, the camera system scans the road, detects the lanes and the land markers [17]. As a result, the absolute positions of the lane boundaries can be determined and used to constrain the filtered/fused outputs. Contrarily to most common map matching approaches, which simply project the vehicle’s position on the center of the road or lane [18], we consider a more realistic

⁹In this case, the Kalman gain depends on the uncertainties of the ‘‘ego’’ predicted state and V2V range measurements.

Algorithm 1 Modified EKF (iteration k , ‘‘ego’’ vehicle i)

- 1: **CAM Collection:** Receive CAMs from the set $\mathcal{N}_{\rightarrow i,k}$ of perceived neighbors, exact the Gaussian beliefs $\{\tilde{\mathbf{X}}_{j,k}, \mathbf{P}_{j,k}\}$, the timestamps $t_{j,k}$ and (optionally) mobility parameters like \mathbf{Q}_j , $j \in \mathcal{N}_{\rightarrow i,k}$.
- 2: **Prediction and Data Synchronization:** Perform prediction of both ‘‘ego’’ and neighboring beliefs based on mobility prediction models at the ‘‘ego’’ estimation instant $t_{i,k}$

$$\begin{aligned} \hat{\mathbf{X}}_{i,k|k-1}^a &= \tilde{\mathbf{F}}^a(\Delta T) \hat{\mathbf{X}}_{i,k-1}^a, \\ \mathbf{P}_{i,k|k-1}^a &= \tilde{\mathbf{F}}^a(\Delta T) \mathbf{P}_{i,k-1}^a \tilde{\mathbf{F}}^a(\Delta T)^\dagger + \tilde{\mathbf{G}}^a(\Delta T) \tilde{\mathbf{Q}}_i^a \tilde{\mathbf{G}}^a(\Delta T)^\dagger, \\ \tilde{\mathbf{X}}_{j,k_i|k} &= \tilde{\mathbf{F}}(\Delta T_k^{i,j}) \tilde{\mathbf{X}}_{j,k}, \\ \mathbf{P}_{j,k_i|k} &= \tilde{\mathbf{F}}(\Delta T_k^{i,j}) \mathbf{P}_{j,k} \tilde{\mathbf{F}}(\Delta T_k^{i,j})^\dagger + \tilde{\mathbf{G}}(\Delta T_k^{i,j}) \tilde{\mathbf{Q}}_j \tilde{\mathbf{G}}(\Delta T_k^{i,j})^\dagger, \\ \Delta T_k^{i,j} &= t_{i,k} - t_{j,k}, \quad j \in \mathcal{N}_{\rightarrow i,k}. \end{aligned}$$

- 3: **Correction:** Select the subset $\mathcal{S}_{\rightarrow i,k} \subset \mathcal{N}_{\rightarrow i,k}$ of paired ‘‘virtual anchors’’ and aggregate the predicted states $\tilde{\mathbf{X}}_{j,k_i|k}$ and covariance matrices $\mathbf{P}_{j,k_i|k}$, $j \in \mathcal{S}_{\rightarrow i,k}$ (by constructing block diagonal matrix) to obtain $\hat{\mathbf{X}}_{\mathcal{S} \rightarrow i,k|k-}$ and $\mathbf{P}_{\mathcal{S} \rightarrow i,k|k-}$ respectively then

$$\begin{aligned} \hat{\mathbf{X}}_{i \cup \mathcal{S},k|k-} &= (\hat{\mathbf{X}}_{i,k|k-1}^\dagger, \hat{\mathbf{X}}_{\mathcal{S} \rightarrow i,k|k-}^\dagger)^\dagger, \\ \mathbf{P}_{i \cup \mathcal{S},k|k-} &= \begin{pmatrix} \mathbf{P}_{i,k|k-1}^a & \mathbf{0} \\ \mathbf{0} & \mathbf{P}_{\mathcal{S} \rightarrow i,k|k-} \end{pmatrix}, \\ \boldsymbol{\nu}_{i,k} &= \mathbf{z}_{i,k} - \mathbf{h}_{i,k}(\hat{\mathbf{X}}_{i \cup \mathcal{S},k|k-}), \\ \mathbf{H}_{i,k} &= \frac{\partial \mathbf{h}_{i,k}}{\partial \mathbf{X}_{i \cup \mathcal{S},k}} \Big|_{\mathbf{X}_{i \cup \mathcal{S},k} = \hat{\mathbf{X}}_{i \cup \mathcal{S},k|k-}}, \\ \mathbf{S}_{i,k} &= \mathbf{H}_{i,k} \mathbf{P}_{i \cup \mathcal{S},k|k-} \mathbf{H}_{i,k}^\dagger + \mathbf{R}_{i,k}, \\ \mathbf{K}_{i,k} &= \mathbf{P}_{i \cup \mathcal{S},k|k-} \mathbf{H}_{i,k}^\dagger \mathbf{S}_{i,k}^{-1}, \\ \hat{\mathbf{X}}_{i \cup \mathcal{S},k} &= \hat{\mathbf{X}}_{i \cup \mathcal{S},k|k-} + \mathbf{K}_{i,k} \boldsymbol{\nu}_{i,k}, \\ \mathbf{P}_{i \cup \mathcal{S},k} &= (\mathbf{I} - \mathbf{K}_{i,k} \mathbf{H}_{i,k}) \mathbf{P}_{i \cup \mathcal{S},k|k-}, \\ \hat{\mathbf{X}}_{i,k} &= [\hat{\mathbf{X}}_{i \cup \mathcal{S},k}]_{1:4}, \quad \mathbf{P}_{i,k} = [\mathbf{P}_{i \cup \mathcal{S},k}]_{1:4,1:4}. \end{aligned}$$

- 4: **Belief Encapsulation and Broadcast:** Encapsulate the fused belief $\{\hat{\mathbf{X}}_{i,k}, \mathbf{P}_{i,k}\}$ and its timestamp $t_{i,k}$ in a CAM and broadcast.

approach called *density truncation*. In this method, the EKF posterior density is truncated at the lane boundaries considered as state constraints. It can be done either analytically [18] or making numerical approximations [9]. Following by the latter approach (due to analytic tractability in our context), we first draw samples from the EKF posterior density. Then samples outside a drivable area are removed. Finally, the constrained density (still assumed Gaussian) is constructed based on the valid samples on the occupied lane, as illustrated in Fig. 3. This truncated density is used to calculate the filter output and reinjected into the next filter iteration. Note that this technique is not entirely appropriate when vehicle changes lanes and the new lane has not been updated yet shortly after the transition. In other words, the error may increase during the short period.

IV. PERFORMANCE EVALUATION

A. Simulation Scenarios

In our MATLAB-based evaluations, we model a horizontal two-lane highway, where 7 ITS-G5 connected vehicles endowed with IR-UWB ranging capabilities are driving steadily in a common direction at the average speed of 110 km/h (i.e., about 30 m/s) for 60 seconds, as shown in Fig. 4. In this

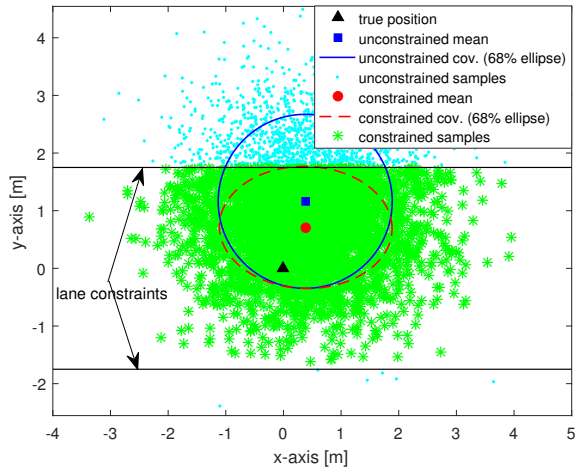


Fig. 3. Example of unconstrained (partially violating lane constraints) vs. constrained (satisfying lane constraints) positional beliefs. The latter reduces noticeably the y -axis (cross-track) error.

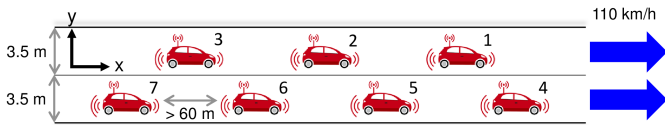


Fig. 4. Evaluated VANET and related attributes in highway scenario.

TABLE I
MAIN SIMULATION PARAMETERS

Parameter	Value
Memory level α	0.95
Along-track acceleration noise (1σ)	1 [m/s ²]
Cross-track acceleration noise (1σ)	0.1 [m/s ²]
Sampling period ΔT	0.1 [s]
Process noises (prediction)	2 [m/s ²]
GNSS position noises (1σ)	3.6 [m] (SPS ^a) [19]
GNSS refresh rate	10 [Hz]
CAM rate	10 [Hz] (critical)
IR-UWB ranging rate	5 [Hz] (hypothesis)
IR-UWB ranging noise (1σ)	0.2 [m]
Gyroscope bandwidth	50 [Hz] [17]
Gyroscope signal noise at 50-Hz bandwidth (1σ)	0.1 [deg/s] [17]
Integrated time span (angle random walk)	0.1 [s]
Lane width	3.5 [m]

^a Standard Positioning Service.

scenario, along-track and cross-track directions coincide with x - and y -axes respectively. The main simulation parameters are summarized in Table I.

B. Simulation Results

Figure 5 compares the errors along x - and y -axes for different fusion strategies by means of empirical Cumulative Distribution Functions (CDFs). Regarding x -axis location errors on Fig. 5(a), as expected, using the IMU or LCs has no or only little impact on the along-track positioning error. Specifically, GNSS, GNSS+IMU, and GNSS+LC schemes yield comparable error levels. Besides, GNSS+UWB+IMU, GNSS+UWB+LC, and all-in-one (GNSS+UWB+IMU+LC) schemes surprisingly suffer from slight accuracy degradation in comparison with GNSS+UWB. This observation can

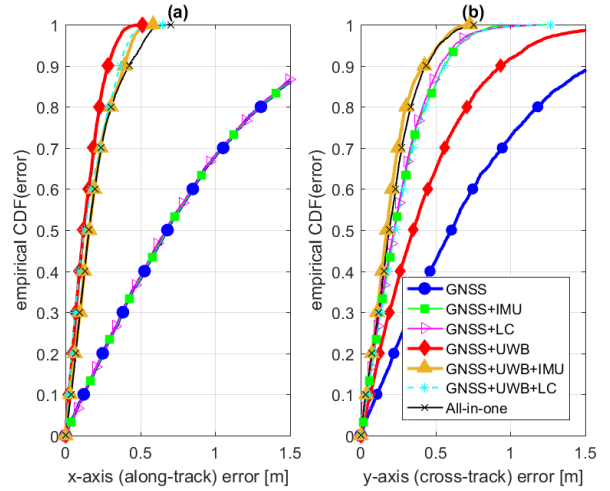


Fig. 5. Empirical CDF of x -axis (along-track/left) and y -axis (cross-track/right) errors for different fusion schemes.

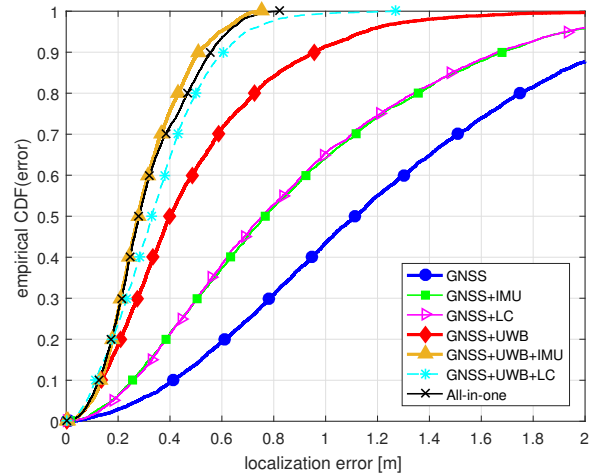


Fig. 6. Empirical CDF of overall localization errors for different fusion schemes.

be explained by considering the effect of y -axis errors on Fig. 5(b). More particularly, due to large y -axis errors within the GNSS+UWB scheme, i.e., 0.35 m and 0.94 m of median and worst-case (WC) (defined for a CDF of 90%) errors respectively, an “ego” vehicle may suffer from singular GDoP. In this case, there exist several neighbors whose relative vectors from an “ego” vehicle are nearly aligned with the road. Accordingly, these misplaced anchors accidentally contribute to improve performance on the along-track axis, whereas they tend to increase the error along the cross-track direction (See again Section III-A or Fig. 2). Fig. 5(a) also reveals that the all-in-one solution is slightly worse than GNSS+UWB+IMU in the large error region. Because the latter is already rather accurate along both x - and y -axes, the density truncation may slightly alter the posterior and be counterproductive.

The performance along the critical y -axis is summarized in Fig. 5(b). As expected, IMU-based heading measurement and LC integration both contribute to dramatically decrease the error. It also confirms the limited impact of range-based CLoc on the cross-track error in poor GDoP VANETs i.e.,

TABLE II
OVERALL PERFORMANCE COMPARISON OF DIFFERENT FUSION SCHEMES

Fusion scheme	x -axis (along-track) error				y -axis (cross-track) error				localization error		
	Med. [m]	WC [m]	CDF(0.2 m)	Gain ^b	Med. [m]	WC [m]	CDF(0.2 m)	Gain ^a	Med. [m]	WC [m]	Gain ^a
GNSS	0.68	1.65	16%	–	0.61	1.55	18%	–	1.11	2.09	–
GNSS+IMU	0.68	1.65	16%	0%	0.23	0.56	44%	62.3%	0.77	1.68	30.6%
GNSS+LC	0.67	1.63	16%	1.5%	0.22	0.53	46%	63.9%	0.76	1.66	31.5%
GNSS+UWB	0.12	0.28	73%	82.4%	0.35	0.94	31%	42.6%	0.40	0.96	64.0%
GNSS+UWB+IMU	0.16	0.40	61%	76.5%	0.17	0.43	58%	72.1%	0.28	0.51	74.8%
GNSS+UWB+LC	0.13	0.37	65%	80.9%	0.23	0.56	44%	62.3%	0.33	0.61	70.3%
All-in-one	0.16	0.43	61%	76.5%	0.19	0.44	52%	68.9%	0.28	0.56	74.8%

^a Relative gain w.r.t. standalone GNSS solution in median error (i.e., CDF = 50%).

with a relative drop by only 42.6% in terms of median error (compared to GNSS) versus 62.3% and 63.9% with non-CLoc schemes such as GNSS+IMU and GNSS+LC respectively. The GNSS+UWB+IMU scheme provides better y -axis accuracy than GNSS+IMU (with relative decreases of 62.3% and 72.1% in terms of median errors respectively) due to the cooperation with several neighbors on the different lanes. The integration of IMU and LC yields comparable accuracy levels when considered in non-CLoc schemes (with relative drops by 62.3% and 63.9% in terms of median error respectively) whereas IMU outperforms LC within CLoc schemes (with relative drops by 72.1% and 62.3% respectively). The first observation is mainly due to the settings e.g., the gyroscope signal noise, the integrated timespan, the lane width, etc. For the second remark, the cross-track error in CLoc is partly improved by some neighbors on other lanes as aforementioned. Thus, the density truncation becomes slightly less effective. Note that the all-in-one option remains still slightly less accurate than GNSS+UWB+IMU in terms of y -axis error.

Finally, Fig. 6 compares the performance of different schemes in terms of 2-D localization (distance) error and confirms the significant accuracy gains offered by the IMU and the LC information. The overall performance comparison is also summarized in Table II for critical error regimes.

V. CONCLUSION AND FUTURE WORK

We studied the problem of range-based CLoc in VANETs in the presence of poor cross-track GDoP caused by constrained vehicular mobility. Simulation results clearly indicate that cross-track positioning errors cannot be fully mitigated through conventional range-based cooperation. We solve this problem by additionally integrating the vehicle's heading information issued at IMUs or contextual information such as lane occupancy and boundaries. The proposed EKF-based data fusion framework is shown to remove unbounded noise (at gyroscopes) and can incorporate inequality constraints onto posterior densities to achieve robust and accurate location estimation. Future works will investigate the case of GNSS-denied environments and road side units. Experimental validations should also be conducted based on real hardware platforms.

ACKNOWLEDGMENT

This work has been performed in the frame of the *HIGHTS* project, which is funded by the European Commission

(636537-H2020). EURECOM acknowledges the support of its industrial members, namely, BMW Group, IABG, Monaco Telecom, Orange, SAP, ST Microelectronics, and Symantec.

REFERENCES

- [1] G. M. Hoang, B. Denis, J. Härrri, and D. T. M. Slock, "Breaking the gridlock of spatial correlations in GPS-aided IEEE 802.11p-based cooperative positioning," *IEEE Trans. on Veh. Technol.*, vol. 65, Dec. 2016.
- [2] N. Drawil and O. Basir, "Intervehicle-communication-assisted localization," *IEEE Trans. on Intel. Transp. Syst.*, vol. 11, pp. 678–691, Sept. 2010.
- [3] G. M. Hoang, B. Denis, J. Härrri, and D. T. M. Slock, "Select thy neighbors: Low complexity link selection for high precision cooperative vehicular localization," in *Proc. VNC'15*, pp. 36–43, Dec. 2015.
- [4] R. Parker and S. Valaee, "Vehicular node localization using received-signal-strength indicator," *IEEE Trans. on Veh. Technol.*, vol. 56, pp. 3371–3380, Nov. 2007.
- [5] G. M. Hoang, B. Denis, J. Härrri, and D. T. M. Slock, "Cooperative localization in GNSS-aided VANETs with accurate IR-UWB range measurements," in *Proc. WPNC'16*, Oct. 2016.
- [6] J. Yao, A. Balaci, M. Hassan, N. Alam, and A. Dempster, "Improving cooperative positioning for vehicular networks," *IEEE Trans. on Veh. Technol.*, vol. 60, pp. 2810–2823, Jul. 2011.
- [7] "Intelligent Transport Systems (ITS); Vehicular Communications; Basic Set of Applications; Part 2: Specification of Cooperative Awareness Basic Service," *ETSI Std. EN 302 637-2 V1.3.2*, Oct. 2014.
- [8] Z. Sahinoglu, S. Gezici, and I. Gvenc, *Ultra-wideband Positioning Systems: Theoretical Limits, Ranging Algorithms, and Protocols*. New York, NY, USA: Cambridge Univ. Press, 2011.
- [9] N. Mattern, M. Obst, R. Schubert, and G. Wanielik, "Co-operative vehicle localization algorithm - Evaluation of the CoVeL approach," in *Proc. SSD*, pp. 1–5, Mar. 2012.
- [10] J. Härrri, C. Bonnet, and F. Filali, "The challenges of predicting mobility," Tech. Rep. 2240, EURECOM, Aug. 2006.
- [11] P. Groves, *Principles of GNSS, Inertial, and Multisensor Integrated Navigation Systems*. Boston-London, UK: Artech House, 2nd ed., 2013.
- [12] M. Maman, B. Denis, M. Pezzin, B. Piaget, and L. Ouvry, "Synergetic MAC and higher layers functionalities for UWB LDR-LT wireless networks," in *Proc. ICUWB'08*, vol. 3, pp. 101–104, Sept. 2008.
- [13] I. P. Prikhodko, S. A. Zotov, A. A. Trusov, and A. M. Shkel, "What is mems gyrocompassing? Comparative analysis of maytagging and carouseling," *J-MEMS*, vol. 22, pp. 1257–1266, Dec. 2013.
- [14] M. Grewal and A. Andrews, "How good is your gyro [ask the experts]," *IEEE Cont. Syst. Mag.*, vol. 30, pp. 12–86, Feb. 2010.
- [15] O. J. Woodman, "An introduction to inertial navigation," Tech. Rep. UCAM-CL-TR-696, Univ. Cambridge, Comp. Lab., 2007.
- [16] R. Neul *et al.*, "Micromachined angular rate sensors for automotive applications," *IEEE Sens. J.*, vol. 7, pp. 302–309, Feb. 2007.
- [17] "D5.2 - Specifications of implemented cooperative and fusion algorithms," *HIGHTS Deliverable*, Aug. 2016.
- [18] D. Simon, *Optimal State Estimation: Kalman, H Infinity, and Nonlinear Approaches*. Newark, NJ, USA: Wiley, 2006.
- [19] USDOD and NAVSTAR GPS, *GPS Standard Positioning Service (SPS) Performance Standard*, 4th ed., Sep. 2008.